Supplementary Information

Flicker Noise as a Probe of Electronic Interaction at Metal-Single Molecule Interfaces

Olgun Adak[1], Ethan Rosenthal[2], Jeffery Meisner[3], Erick F. Andrade[3]

Abhay Pasupathy[2], Colin Nuckolls[3], Mark S. Hybertsen[4] and Latha Venkataraman[1]

[1]Department of Applied Physics and Applied Mathematics, [2]Department of Physics, and [3]Department of Chemistry, Columbia University, New York, NY

[4]Center for Functional Nanomaterials, Brookhaven National Labs, Upton, NY

Contents:

1. Experimental Set-Up and Analysis of Noise Sources
2. Gold Point Contacts under Mechanical Perturbation
3. Scaling of Flicker Noise in Tunnel Junctions
4. Scaling of Flicker Noise in Gold Nanoscale Contacts
5. Voltage Dependence of Flicker Noise
6. DFT Calculation Details
7. Scaling of Flicker Noise in Molecular Junctions
8. Model for Scaling of Flicker Noise Power in Molecular Junctions
9. Rotations and Rupture of the Au-S Linker Bond
10. References

1. Experimental Set-Up and Analysis of Noise Sources

a. The Experimental Set-up:

The block diagram of the room temperature experimental setup is shown in Figure S1A. A voltage is applied to the junction using a digital to analog converter (NI PXI-4461), while the current through the junction is converted to voltage using a transimpedance amplifier (Keithley 428-PROG and Femto DLPCA-200). The voltage output of the transimpedance amplifier and the voltage across the junction are recorded at 100 kHz using A/D inputs on the NI PXI-4461. A resistor (R_s) is placed in series with the junction to prevent an overload in the transimpedance amplifier when the junction resistance is low. Neither the transimpedance amplifier nor the data acquisition card have a 1/f noise comparable to what we measure for the junctions. Mechanical perturbations to our setup are damped above 5 Hz by a two-stage vibration isolation system. The resonance frequency of our piezoelectric transducer is around 10 kHz.

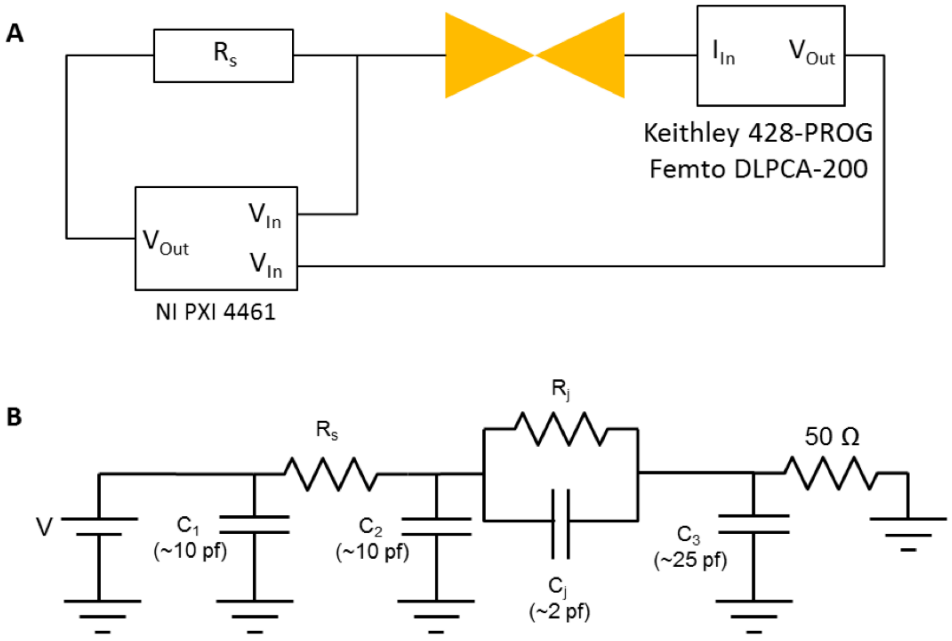

Figure S1. (A) Block diagram of STM-BJ circuitry used for both room temperature and low-temperature measurements. (B) Details of the circuit showing all resistances and capacitances.

Figure S1B shows the circuit diagram: C_1, C_2, C_3 are the cable capacitances, C_j denotes the junction capacitance. The transimpedance amplifier has a 50 Ω input impedance. Since any

current that passes through C_1 does not go through the junction, C_1 does not affect the measured current. Although C_2 has an impedance comparable to the junction impedance at 1 kHz, it does not affect the conductance measurement since the junction conductance is obtained by dividing the measured current through the junction by the measured voltage across the junction. C_3 is in parallel with the transimpedance amplifier. At 1 kHz, the impedance of C_3 is 6.4×10^6 Ω which is not comparable to 50 Ω input impedance of the amplifier thus C_3 does not affect the measurement. The effect of C_j on conductance measurement depends on R_s. In the absence of the series resistor, C_j does not affect the DC conductance measurement. However, when the series resistor is present, the voltage across the junction changes with the junction resistance, which involves charging or discharging of C_j. From the RC time constant for this capacitor (with R_s = 100 kΩ) we see that frequency beyond which these capacitive effects matter is 1 MHz, well above the range used here, thus the junction capacitance not does limit the measurements presented here. For experimental verification, we obtain the transfer function within the measurement bandwidth by measuring the current through the circuit while applying a white voltage noise when the gold tip is in contact with the substrate. The transfer function within 100 Hz to 1 kHz bandwidth is flat and equal to 1 as shown in Figure S2A.

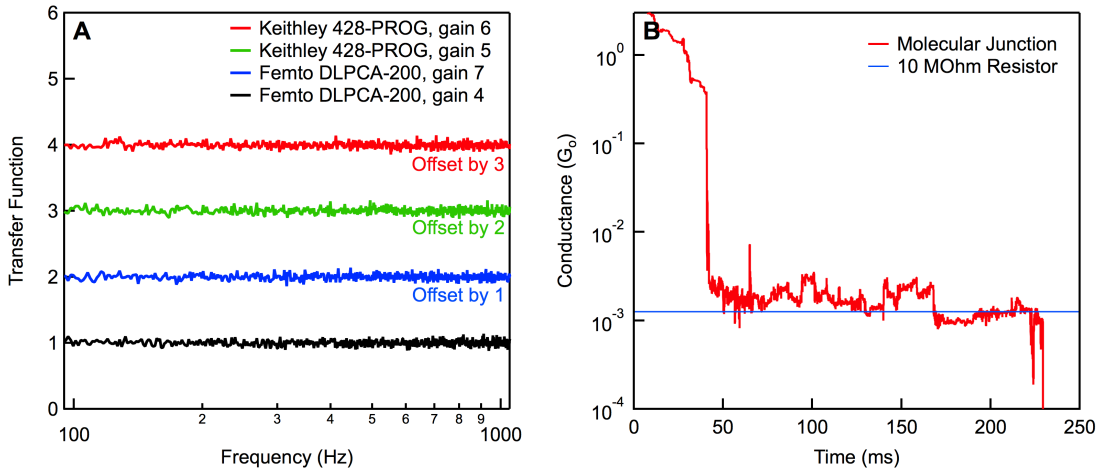

Figure S2. (A) The transfer functions of the experimental setup within the experimental bandwidth. The traces are offset vertically for clarity. (B) Comparison of conductance of 10 MOhm resistor and a molecular junction measured with the experimental set-up showing that the instrument noise is negligible.

b. Analysis of Additional Noise Sources:

The additional noise sources can be divided into two categories: instrumental and physical noise. The former contains noise due to the current to voltage (IV) converter, the voltage probe and the voltage source. The latter contains shot noise and thermal noise.

Room Temperature Measurements:

The total measured instrumental conductance noise within the measurement bandwidth (100-1000 Hz) is 3.4×10^{-13} G_0^2 for tunnel junction and molecular junction measurements at room temperature. This is measured using a NI-PXI 4461 voltage probe, a Keithley 428-PROG gain 10^6 IV converter under a bias voltage of 200 mV applied using the NI-PXI 4461 card. The instrumental conductance noise for the gold point contact at room temperature is 4.4×10^{-11} G_0^2. This is measured using a NI-PXI 4461 voltage probe, a Femto DLPCA-200 gain 10^5 IV converter under a bias voltage of 50 mV applied using the NI-PXI 4461 card. These values are at least two orders of magnitude smaller than the flicker noise measured for the corresponding junction (see Figure 2B, SI Figure S5 and S6) thus instrumental noise is clearly not significant. The manufacturer reported noise in the voltage source is less than 8.5×10^{-15} [V^2Hz^{-1}] and not measureable with the voltage probe. The corresponding conductance noise in each system is orders of magnitudes less than the instrumental noise originating from the IV converters and the voltage probe, and is therefore insignificant. In Figure S2B, we compare the conductance of a 10 MOhm resistor and a molecular junction measured with the same set-up where it is clear that the instrument noise is negligible.

The thermal current noise of a junction is given by $4k_bT/R$ [A^2/Hz]. The corresponding conductance noise is $4.8\times10^{-12}/G$ [G_0^2] for molecular junctions and tunnel junctions measured under 200 mV DC bias, and $7.7\times10^{-11}/G$ [G_0^2] for gold point contacts measured under 50mV DC bias, where G is in the units of G_0. These numbers are orders of magnitudes smaller than the instrumental noise for the corresponding junctions and can safely be neglected. Shot noise in gold point contacts is even smaller than the thermal noise at room temperature, and requires lock-in type measurements and RF amplifiers.[1,2] To date, shot noise in molecular junctions and tunnel junctions at room temperature has not been measured. Therefore, our flicker noise measurements at room temperature are clearly orders of magnitude above any instrumental noise and much larger than other noise of physical origin.

Low Temperature Measurements:

The measured instrumental conductance noise density at 100 Hz is 2.8×10^{-17} [G_0^2/Hz] for tunnel junction low temperature measurements. This is measured using a NI-PXI 4461 voltage probe, a Femto DLPCA-200 gain 10^7 IV converter under a bias voltage of 100 mV applied using the NI-PXI 4461 card. The measured instrumental conductance noise density at 100 Hz is 5.0×10^{-12} [G_0^2/Hz] for gold point contact measurements at 77 K. This is measured using a NI-PXI 4461 voltage probe, a Femto DLPCA-200 gain 10^4 IV converter under a bias voltage of 50 mV applied using the NI-PXI 4461 card. These values are obtained by measuring the conductance noise after the corresponding junction ruptures. This noise is primarily due to the thermal noise in the IV converters. In the analysis of tunnel junctions, the noise power density is normalized by the square of conductance to remove conductance dependence. The contribution to measured normalized noise from the instrumental noise floor is 2.8×10^{-10} [Hz^{-1}] for junctions with a conductance of $10^{-3.5}G_0$ and 2.8×10^{-14} [Hz^{-1}] for junctions with a conductance of $10^{-1.5}G_0$. These values are much smaller than the normalized conductance noise measured in our experiments as shown in Figure 4B and SI Figure S4B. The thermal noise in all systems is smaller than the room temperature thermal noise, while shot noise temperature independent. Thus, the thermal noise and shot noise are orders of magnitudes smaller than the instrumental noise. The primary source of signal observed at low temperatures in the absence of two-level fluctuations is due to the drifts in piezoelectric transducer rather than the instrumental noise or noises of physical origin. We note that the drift induced noise is insignificant compared to the noise measured at room temperature.

2. Gold Point Contacts under Mechanical Perturbation

To probe the relation between the flicker noise and the mechanical stability of a gold point contact, an AC oscillation at 10 kHz with amplitude around 0.1 nm is applied to the tip during the noise measurement. The conductance change due to mechanical perturbation is determined from the AC component of the conductance at 10 kHz.

In Figure S3A, we show the conductance change due to AC oscillation of the tip at 10 kHz against the average conductance for 50000 gold point contacts as a two-dimensional histogram. We see dips at conductance values slightly lower than the integer multiples of G_0 similar to what was seen in Figure 2A of the manuscript. The 10 kHz conductance

change scales with $G^{0.6}$ above 4 G_0, again similar to what is seen in Figure 2A ($G^{0.5}$) indicating that the atoms on the periphery of the junction are primarily responsible for the change in conductance upon mechanical perturbation.

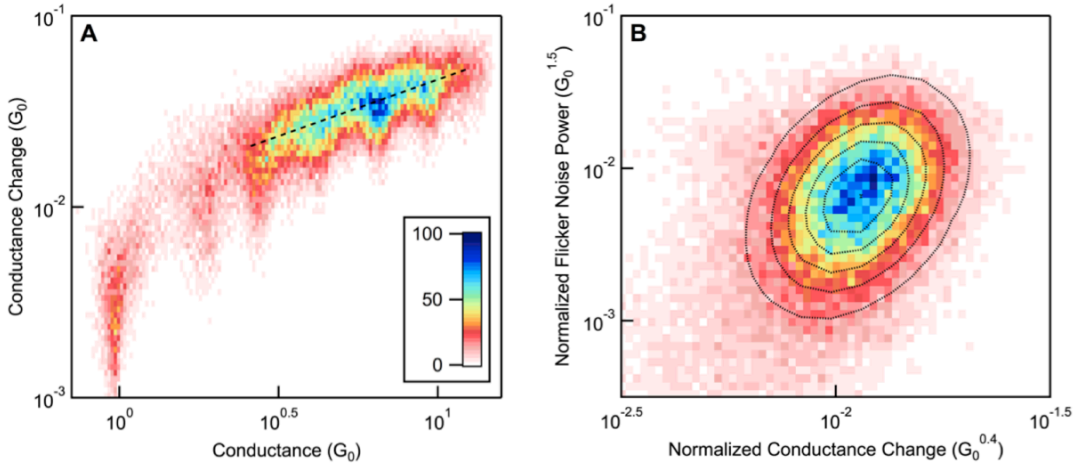

Figure S3. (A) Two-dimensional histogram of conductance change due to mechanical perturbation against average conductance in gold point contacts. (B) Two-dimensional histogram of normalized conductance change due to mechanical perturbation against normalized flicker noise power in gold point contacts.

We show, in Figure S3B the correlation between the flicker noise power normalized by $G^{0.5}$ (from data shown in Figure 3A) and the conductance change due to mechanical perturbations normalized by $G^{0.6}$ (from Figure S3A). The clear correlation seen here demonstrates that junction that are more susceptible conductance change upon mechanical perturbation experience more flicker noise.

3. Scaling of Flicker Noise in Tunnel Junctions

For $G(z) = G_c e^{-bz}$ and a Gaussian distribution of z, $p(z) = \frac{1}{\sqrt{2\pi\sigma^2}} e^{\frac{(z-z_O)^2}{2\sigma^2}}$, the average conductance is

$$< G >= \int_{-\infty}^{\infty} dz\, G_c e^{-bz} \frac{1}{\sqrt{2\pi\sigma^2}} e^{-\frac{(z-z_O)^2}{2\sigma^2}}.$$

Upon integration, this yields:

$$< G >= G_c e^{-bz_o} e^{b^2\sigma^2}.$$

Likewise, for the average of the square of fluctuations,

$$< \Delta G^2 >= \int_{-\infty}^{\infty} dz\, G_c^2 e^{-2bz} \frac{1}{\sqrt{2\pi\sigma^2}} e^{-\frac{(z-z_O)^2}{2\sigma^2}} - < G >^2,$$

which yields:

$$< \Delta G^2 >= < G >^2 \left[e^{2b^2\sigma^2} - 1\right],$$

which clearly shows the noise power is proportional to the $<G>^2$.

4. Scaling of Flicker Noise in Gold Nanoscale Contacts

The conductance of a gold nanoscale contact is approximately one unit of G_0 per atom in the contact cross-section area. Fluctuations due to Au atom motion take place at the edge of the contact area, so the number of possible sites subject to fluctuations should scale with the circumference of the junction, assuming these sites are accessible to diffusing atoms. While junctions that approach a single atom scale may be physically less accessible due to mechanical elongation and deformation, junctions above a certain conductance or area should have an accessible circumference. We assume that the flicker noise is the net effect of independent events where each available site around the circumference can host a fluctuating, two-level system. Then the flicker noise power, which scales as the number of two-level systems, is proportional to the square root of the conductance.

5. Voltage Dependence of Flicker Noise

There are two possible mechanisms for noise increase with bias voltage; a local heating of the junction due to loss of electron energy by scattering that excites vibrations or a lowering of potential barrier for atom movement on the electrodes.[3-5] In order to distinguish between the two different mechanisms, we measure the conductance noise in tunnel junctions at voltages ranging from 100mV to 500mV with conductance ranging from $10^{-1.4}$ G_0 to 10^{-4} G_0. In Figure S4A, red and blue circles points show the voltage dependence of conductance noise power density at 100 Hz at 5.5 K with conductance $10^{-2 \pm 0.5}$ and $10^{-3 \pm 0.5}$ respectively. Dots represent the measured values, empty circles represent the values after background subtraction. As stated in the manuscript, for all low-temperature data, we choose to take the noise density at 100 Hz instead of integrating from 100 Hz to 1 kHz to minimize impact from external noise in the set-up. If the increase in the noise is due to a local heating of the electrodes, the average local temperature of junctions can be determined from the temperature dependence of the low-bias flicker noise measurements (e.g., the green trace in Figure 3B). Under a 0.5 V bias, junctions with conductance $10^{-2 \pm 0.5}$

and $10^{-3 \pm 0.5}$ G_0 have a noise power density of 3.7×10^{-07}/Hz and 1.4×10^{-07}/Hz respectively, which in view of the exponential dependence of noise on temperature in Figure 3B, would imply a very modest difference in temperature (~25 K). However, these junctions differ in conductance by an order of magnitude, and in general, one would expect that local heating, which should scale approximately as GV^2, would be significantly higher for higher conductance junctions. Therefore a local heating effect cannot explain the voltage-induced noise measured here. We also see that the noise increases exponentially with the applied voltage. This indicates that the voltage effectively decreases the barrier for atomic motion on the electrode surfaces, yielding a modified two-level system as detailed by Muller and coworkers.[6]

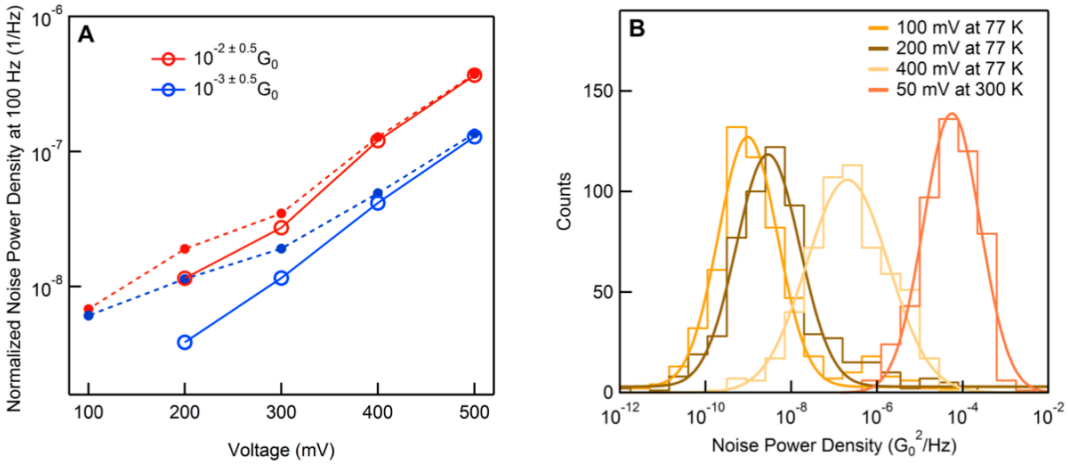

Figure S4. (A) The noise power density at 100 Hz normalized by the square of the average junction conductance plotted against bias voltage in tunnel junctions with average conductance around $10^{-2\pm0.5}$ G_0 (red) and $10^{-3\pm0.5}$ G_0 (blue). Dots represent the measured values, empty circles represent the values after background subtraction. (B) Histograms for the conductance noise power density at 100 Hz in gold point contacts with a conductance ranging between 3 G_0 and 6 G_0.

In gold point contacts, at 77 K, we do not see switching events under 50 mV bias voltage. However, as we increase the bias, conductance fluctuations are observed as shown in Figure S4B as the noise density is increasing above the experimental noise floor obtained at 50 mV bias voltage.

6. DFT Calculation Details

For the DFT studies, model structures were developed based on a 3 monolayer (ML) slab of gold atoms modeling a close-packed (111) surface, with different adatom

superstructures added on one side and a minimum of 10A of vacuum separation. The back two ML were held fixed at distances according to the cubic lattice parameter of a=4.175A, determined from the optimized bulk lattice parameter computed under the present computational conditions (PAW method with the PBE function, 400 eV energy cut-off to determine the planewave basis set size and a uniform, G-centered mesh of k-points with 15 points in each direction to sample the Brillouin zone). Surface supercells with area 3×3, 4×4 and 5×5 relative to the basic hexagonal unit cell were considered, giving different degrees of separation between periodic replicas of the adatom superstructures. Surface Brillouin sampling was roughly commensurate with 15 k-points in each direction in the bulk. Potential surfaces displayed in Figure 3 were mapped between metastable basins. Initial coordinates were obtained by linear interpolations, followed by relaxation with the x-y coordinates of the adatom under study held fixed. Dipole corrections were included for test structures, but found to have no appreciable impact on the energy differences reported here (1 meV scale). All of the results reported in Figure 3C were obtained with 4×4 supercells. The basic energies characterizing adatom diffusion (hcp to fcc hollow energy difference [32, 49, 55 meV] and bridge site barrier from the fcc hollow [129, 140, 143 meV]) depend only weakly on super cell size (3×3, 4×4 and 5×5, respectively). However, the potential pathway for separation of an atom away from a larger superstructure, such as dissociation of the 5 atom structure in Figure 3E into a 4 atom pyramid and a separated adatom, show larger variations with supercell size. In particular, with an increase to a 5x5 cell, the relative energy of the structure with the separated adatom increased from 370 to 460 meV in the first hcp metastable site and from 370 to 450 meV in the next fcc metastable site. Periodic replicas are close enough to influence the energetics, largely due to strain effects. Direct estimates of electrostatic dipole effects were much smaller. Overall, since our purpose is to illustrate scenarios and the real surfaces under study are likely rough, such variations largely serve to underscore the diversity of energy barriers that govern Au atomic rearrangements under realistic conditions.

7. Scaling of Flicker Noise in Molecular Junctions

In the top panel of Figure S5, we show two-dimensional histograms of flicker noise power against conductance. A power-law dependence between these observables is seen in these figures with noise power being proportional to G^n where n is the scaling exponent.

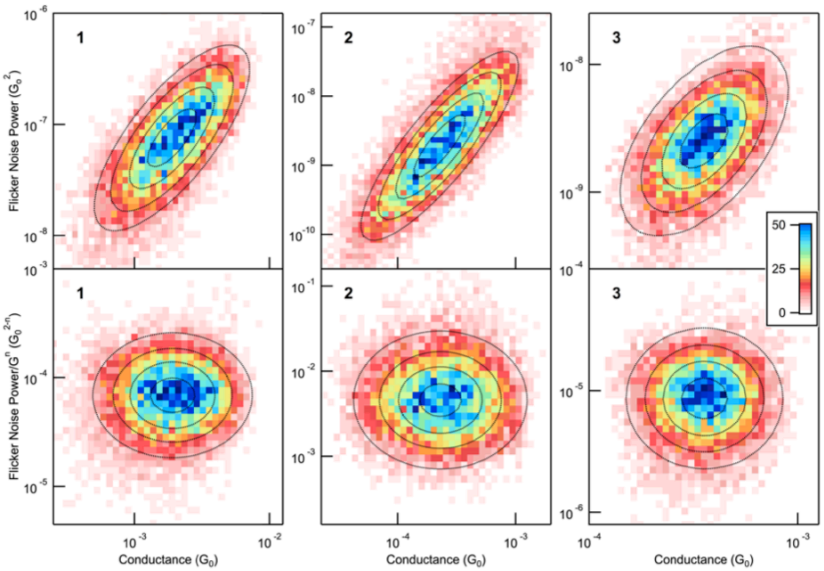

*Figure S5. (Top) Two-dimensional histograms of flicker noise power against average conductance for molecules **1**, **2,** and **3** respectively. (Bottom) Two-dimensional histograms of flicker noise power normalized by $G^{1.1}$, $G^{1.7}$ and $G^{1.0}$ against average conductance for molecules **1**, **2,** and **3** respectively.*

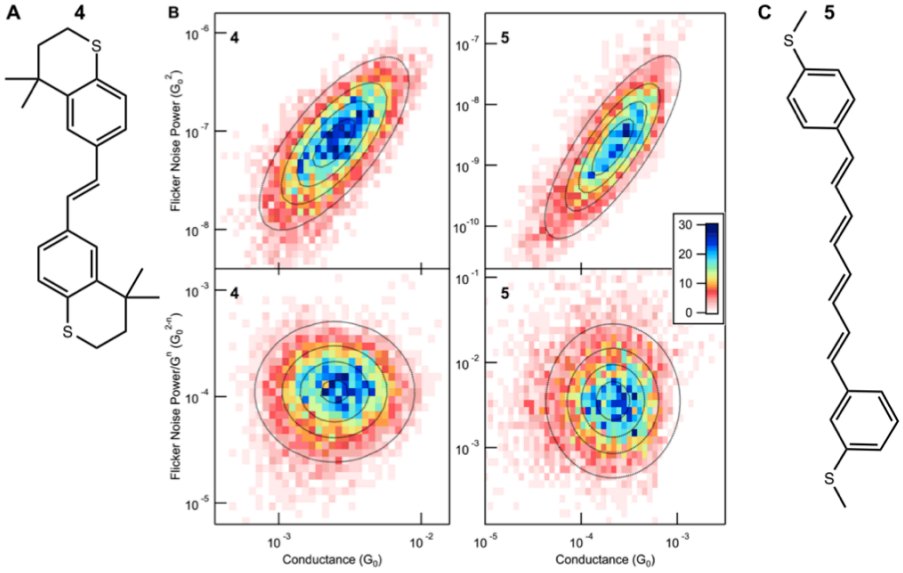

*Figure S6. (A) Chemical structure of **4.** (B) (Top) Two-dimensional histograms of flicker noise power against average conductance for molecules **4** and **5** respectively. (Bottom) Two-dimensional histograms of flicker noise power normalized by $G^{1.2}$ and $G^{1.7}$ against average conductance for molecules **4** and **5** respectively. (C) Chemical structure of **5**.*

In order to determine the scaling exponent, we scale the flicker noise power with G^n using values for n ranging from 0.5 to 2.5 in steps of 0.01. For each n, we obtain the correlation between the normalized flicker noise power and the average conductance by fitting to the bivariate normal distribution. The value of n that leads to zero correlation between the normalized flicker noise power and average conductance is taken as the scaling exponent. Results from this analysis for molecules **1**, **2** and **3** are shown in Figure S5. In addition, we show data for a control through-bond coupled molecule, 1,2-bis(4,4-dimethylthiochroman-6-yl)ethylene (**4**), and a second hybrid molecule with one through-bond and one through-space coupling (**5**) in Figure S6. The synthesis of these compounds are described in Batra et al[7] and Meisner et al.[8] Molecule **4** has a scaling exponent of 1.2 while molecule **5** has a scaling exponent of 1.7.

8. Model for Scaling of Flicker Noise Power in Molecular Junctions

In the simplest physical picture, the transmission function (T(E)) that describes the probability of charge transfer across a molecular junction can be modeled by a Lorentzian function[9] and we have

$$T(E) = \frac{\Gamma_1\Gamma_2}{(E-E_{Frontier})^2+(\Gamma_1+\Gamma_2)^2/4} \qquad (1)$$

where, $E_{Frontier}$ denotes the position of the frontier molecular orbital level relative to the Fermi level (E_F). For low bias measurements, $G=G_0T(E_F)$. Then, in the limit that Γ is much smaller than $E_{Frontier}$, the conductance can be approximated as

$$G = G_0 \frac{\Gamma_1\Gamma_2}{{E_{Frontier}}^2} \qquad (2)$$

Now, while the fluctuations on the two sides of the junction are independent, assume that the average electronic coupling (Γ_{AVG}) and the range of the fluctuations ($\Delta\Gamma$) are the same. Then the fluctuations in conductance can be written as:

$$\Delta G = 2G_{AVG}\frac{\Delta\Gamma}{\Gamma_{AVG}} \qquad (3)$$

where $G_{AVG} = G_0 \frac{{\Gamma_{AVG}}^2}{{E_{Frontier}}^2}$.

In a through-space coupled system, the molecular orbital coupling strength (Γ) decreases exponentially with the distance because Γ is proportional to the overlap between the exponentially decaying tails of the electrode and molecular wavefunctions. The effect of

atomic motion on the electrode (two-level fluctuations) on Γ comes from the modification of the distance between coupling sites, z, as:

$$\Gamma = \mathrm{A}e^{-\beta z} \tag{4}$$

where β is the decay constant and A is a prefactor. This can be written as

$$\Gamma = \mathrm{A}e^{-\beta z_o}e^{-\beta(z-z_o)} \tag{5}$$

where z_o is the average distance between through-space coupled sites.

Similar to the derivation presented in the manuscript for tunnel junction, we get

$$\Gamma = \Gamma_{AVG}\frac{e^{-\beta(z-z_o)}}{<e^{-\beta(z-z_o)>}} \tag{6}$$

where $\Gamma_{AVG} = \mathrm{A}e^{-\beta z_o} < e^{-\beta(z-z_o)} >$.

Therefore, the fluctuations in Γ are proportional to Γ_{AVG}. Assuming both electrodes are coupled through-space to the molecule, we have $\Delta\Gamma/\Gamma_{AVG}$ as a constant and according to eq. (3), we find that $\Delta G \propto G_{AVG}$. Therefore, the flicker noise power should scale with ${G_{AVG}}^2$ in a system with only through-space electronic coupling at the electrodes. This is parallel to the vacuum tunneling case already considered.

When the electronic coupling is through-bond, the mechanical bond (Au-S donor-acceptor in the cases under study here) puts constraints on the bond length and other geometrical factors, such as bond and backbone orientation that influence the electronic coupling. The adjacent electrode structure including the Au atomic organization around the point of contact Au atom, also affects the electronic coupling.[10] If we consider the ensemble of junctions, all of these factors change with each junction in the ensemble resulting in a distribution of electronic coupling and conductance. However, in a given junction, we hypothesize that the primary source of fluctuations is confined to the Au atomic organization. Therefore, we expect the range of the dynamical fluctuations (ΔΓ) to be independent of the average value for a given junction (Γ_{AVG}), as born out by explicit simulations.[10] In this case, following the derivation above, we get:

$$\Delta G = G_0^{0.5}G_{AVG}^{0.5}\Delta\Gamma/E_{Frontier}$$

Since $\mathrm{E}_{\mathrm{Frontier}}$ depends only weakly on Γ,[10] the flicker noise magnitude scales with $G_{AVG}^{0.5}$, hence the flicker noise power scales with G_{AVG} in such a system.

To understand the behavior of a hybrid system, we consider a single molecular level connected to the electrodes by a through bond coupling ($\Gamma_1 = \Gamma_{bond}$) on one side and a through space ($\Gamma_2 = \Gamma_{space}$) coupling on the other. In order to sample the conductance fluctuations, we use Eq. (2) together with a Monte-Carlo simulation in which, for each junction in the ensemble, we pick a value for Γ_{bond} and Γ_{space} assuming lognormal distributions, with the form:

$$f(\Gamma) = \frac{1}{\Gamma\sigma\sqrt{2\pi}} e^{-\frac{(\log(\Gamma/\Gamma_0))^2}{2\sigma^2}} \qquad (7)$$

parameterized by a median value Γ_0 and a standard deviation σ. Here, Γ_0 has units of energy while σ is unit less. This choice is motivated by the experimental observation that logarithmically binned conductance histograms show normal peak distributions. With the approximation of a fixed value of $E_{Frontier}$, this regenerates the conductance distribution. For the simulation discussed below, we consider two such lognormal distributions defined in eq. (7) above, one for each side of the junction with a median value $\Gamma_{0,space}$ and $\Gamma_{0,bond}$ and a corresponding standard deviation σ_{space} and σ_{bond}.

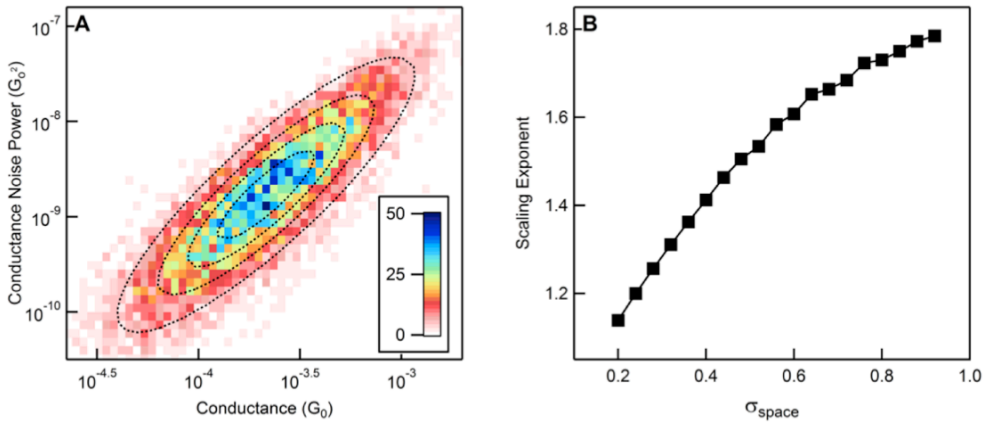

Figure S7. (A) Two-dimensional histogram plot of conductance noise power against average conductance from the Monte Carlo simulation. The parameters used for this simulation are: $\Gamma_{0,bond}$ = 90 meV, $\Gamma_{0,space}$ = 9 meV ,σ_{bond} = 0.47, σ_{space} = 0.74, σ_{noise} = 14 meV. (B) Scaling exponent versus the standard deviation of the through-space coupling strength.

To simulate the conductance fluctuations, we assume that Γ_{bond} varies in time through a white Gaussian noise with zero mean and standard deviation σ_{noise}. This models a fluctuation in Γ_{bond} that is independent of Γ_{bond}. We then assume that Γ_{space} varies in time through a noise that is the product of $\Gamma_{space}/\overline{\Gamma_{bond}}$ and a white Gaussian noise with zero mean and standard deviation σ_{noise}. Γ_{bond}, Γ_{space} and σ_{noise} have units of energy . This allows us

to have a Γ_{space} with fluctuations proportional to Γ_{space}, as detailed above. The factor of $\overline{\Gamma_{bond}}$ is introduced to ensure that when $\Gamma_{space} = \overline{\Gamma_{bond}}$, fluctuations in Γ_{space} are on the same scale with Γ_{bond} since noise source is the same in both cases. Next, conductance traces are calculated by assuming single Lorentzian transmission with conducting molecular orbital located 2 eV away from the Fermi level, though choice of this value is not important since it is just a multiplicative factor relating coupling to conductance. The average conductance and the conductance noise power (the variance of the conductance) are obtained for each trace. This procedure is repeated 10000 times to create a two-dimensional histograms plot of the conductance noise power versus the average conductance as shown in SI Figure S7A. For this simulation, we tune the parameters $\Gamma_{0,bond}$, $\Gamma_{0,space}$, σ_{bond}, σ_{space} and σ_{noise} to model the results of molecule **2** shown in SI

Next, we vary the model parameters to understand how they affect the noise scaling exponent. We find that $\Gamma_{0,bond}$, $\Gamma_{0,space}$ and σ_{noise} do not affect the scaling exponent. However the ratio between σ_{bond} and σ_{space} does control it. To demonstrate this, we fix σ_{bond} at 0.47 and vary σ_{space} from 0.2 to 0.9. We find that the scaling exponent ranges from 1.1 to 1.8 over this range as shown in Figure S7B. For $\sigma_{bond} = \sigma_{space}$, we get an exponent of 1.5. We conclude that the hybrid systems we have studied experimentally have a Γ_{space} that varies more from junction to junction than Γ_{bond}, consistent with the fact that the width of the conductance histogram for **2** is larger than that of **1**.

9. Rotations and Rupture of the Au-S Linker Bond

Rotations about the Au-linker bond: In order to examine the effect of linker rotations on flicker noise in molecular systems, we compare results from measurements of **4** and **1**. Junctions formed with **4** have the orientation of the Au-S bond rigidly locked relative to the terminal benzene rings, while in **1**, this Au-S bond can rotate freely (see Figure S6A for chemical structure).[11] In Figure S8A, we compare the flicker noise power of **1** and **4**, and see that these are very similar. Furthermore, as we have shown, in Figure S6B, flicker noise scales with $G^{1.2}$, which is very similar to the behavior of the other through-bond systems investigated here. We conclude that the rotations about the Au-S bond in **1** do not contribute to the flicker noise measured here.

Rupture and reattachment of the Au-linker bond: Prior DFT calculations indicate that the Au-S bond has a binding energy of about 0.6 eV.[11,12] At room temperature, within the 100

ms experimental timescale, events that involve the linker-Au bond rupture are observable. We find that 10% of molecular junctions do rupture during 100 ms measurement time. These are however not included in our noise analysis, thus the relevant Au-linker bond rupture events that can contribute to the measured noise involve junctions where the bond ruptures and reforms within the 100 ms measurement time. To see how frequently such events are measured, we compare conductance data during the 100 ms section for **1**, **2** and **3** junctions with that of the instrument noise determined after a junction is broken. In Figure S8B, we show histograms of these conductance data and see that there is no overlap in the conductance histograms from traces that are selected for noise measurements and the experimental noise floor. This indicates that a rupture followed by a reattachment process does not happen within 100 ms timescale. We therefore conclude that the measured noise does not result from events involving the Au-S bond rupturing and reforming.

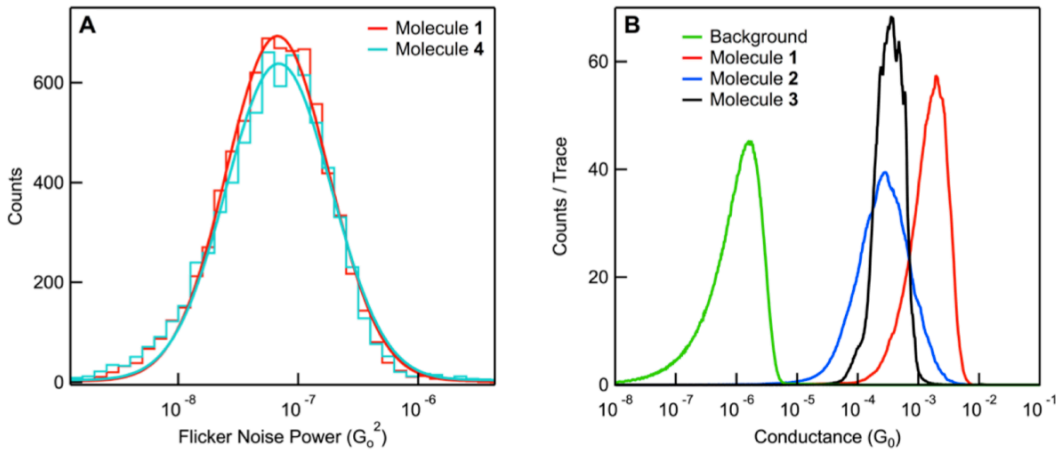

*Figure S8. (A) Histograms of the flicker noise power for molecule **1** and **4**. (B) Conductance histograms compiled from the constant displacement sections of the traces that show molecular junctions at the beginning and end of the constant displacement section for three molecular systems (red, blue, black) and conductance histogram of the experimental background (green), which does not overlap the other histograms.*

10. References:

1 Chen, R., Wheeler, P.J., & Natelson, D., Excess noise in STM-style break junctions at room temperature. *Phys. Rev. B* 85 (23), 235455 (2012).

2 van den Brom, H.E. & van Ruitenbeek, J.M., Quantum Suppression of Shot Noise in Atom-Size Metallic Contacts. *Phys. Rev. Lett.* 82 (7), 1526-1529 (1999).
3 Sperl, A., Kröger, J., & Berndt, R., Direct observation of conductance fluctuations of a single-atom tunneling contact. *Phys. Rev. B* 81 (3), 035406 (2010).
4 Tsutsui, M., Kurokawa, S., & Sakai, A., Bias-induced local heating in atom-sized metal contacts at 77K. *Appl. Phys. Lett.* 90 (13) (2007).
5 Hubert, K., Thomas, L., Remi, Z., Philippe, D., & Andrés, S., Conductance fluctuations in gold point contacts: an atomistic picture. *Nanotechnology* 23 (23), 235707 (2012).
6 Muller, C.J., van Ruitenbeek, J.M., & de Jongh, L.J., Conductance and supercurrent discontinuities in atomic-scale metallic constrictions of variable width. *Phys. Rev. Lett.* 69 (1), 140-143 (1992).
7 Batra, A. *et al.*, Tuning Rectification in Single-Molecular Diodes. *Nano Lett.* 13 (12), 6233-6237 (2013).
8 Meisner, J.S. *et al.*, Importance of direct metal-π coupling in electronic transport through conjugated single-molecule junctions. *J. Am. Chem. Soc.* 134 (50), 20440-20445 (2012).
9 Paulsson, M. & Datta, S., Thermoelectric effect in molecular electronics. *Phys. Rev. B* 67 (24), 241403 (2003).
10 Quek, S.Y. *et al.*, Amine-gold linked single-molecule circuits: Experiment and theory. *Nano Lett.* 7 (11), 3477-3482 (2007).
11 Park, Y.S. *et al.*, Frustrated Rotations in Single-Molecule Junctions. *J. Am. Chem. Soc.* 131 (31), 10820-10821 (2009).
12 Park, Y.S. *et al.*, Contact Chemistry and Single- Molecule Conductance: A Comparison of Phosphines, Methyl Sulfides, and Amines. *J. Am. Chem. Soc.* 129 (51), 15768-15769 (2007).